research papers

JOURNAL OF SYNCHROTRON RADIATION

ISSN 1600-5775

Local atomic structure analysis of GaN surfaces via X-ray absorption spectroscopy by detecting Auger electrons with low energies

Noritake Isomura,* Daigo Kikuta, Naoko Takahashi, Satoru Kosaka and Keita Kataoka

Toyota Central R&D Laboratories Inc., 41-1 Yokomichi, Nagakute, Aichi 480-1192, Japan.
*Correspondence e-mail: isomura@mosk.tytlabs.co.jp

Received 19 July 2019
Accepted 16 September 2019

Edited by R. W. Strange, University of Essex, UK

Keywords: extended X-ray absorption fine structure; Auger electron yields; surface sensitivity; gallium nitride; *K*-shell absorption.

GaN is a promising material for power semiconductor devices used in next-generation vehicles. Its electrical properties such as carrier mobility and threshold voltage are affected by the interface between the oxide and the semiconductor, and identifying the interface states is important to improve these properties. A surface-sensitive measurement of Ga *K*-edge extended X-ray absorption fine structure (EXAFS) by detecting Ga *LMM* Auger electrons that originate from Ga *K*-shell absorption is proposed for GaN. *LMM* Auger electrons with low energies were detected and the EXAFS oscillation was confirmed, providing information on the Ga atoms at the surface. Investigation of thermally oxidized GaN with an oxide film of defined thickness showed that the analysis depth was less than 10 nm, which is consistent with the inelastic mean free path of 2.3 nm estimated for *LMM* Auger electrons in GaN.

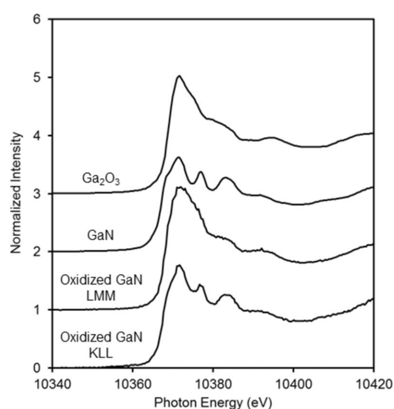

© 2019 International Union of Crystallography

1. Introduction

Presently, the number of electric vehicles is rapidly increasing. A key component of these vehicles is the power semiconductor device, and its efficiency improvement is strongly pursued with the intention of saving energy. To date, Si power devices are being applied widely; however, their performance is limited by several Si-material characteristics. Power devices made using GaN can be operated with higher breakdown voltages, switching speeds and temperatures than devices made using Si (Trivedi & Shenai, 1999). Hence, GaN has a large potential for use in the power semiconductor devices for next-generation vehicles (Kachi, 2014).

In metal-oxide semiconductor field-effect transistors, electrical properties such as carrier mobility and threshold voltage are affected by the interface between the oxide and the semiconductor (Chakroun *et al.*, 2014; Nakano *et al.*, 2003). The factors affecting these properties are not only the interface states but also damages induced by etching during the manufacturing process (Tang *et al.*, 2009; Kim *et al.*, 2012). Therefore, identifying the interface states is important for the improvement of electrical properties.

X-ray absorption spectroscopy, which provides information about local atomic structures, has been widely applied in the study of various materials (Stern & Heald, 1983). In particular, extended X-ray absorption fine-structure (EXAFS) spectroscopy is applied to determine interatomic distances and coordination numbers around target atoms (Teo & Joy, 1980), and the possibility exists that the atomic structure of the interface between oxide and GaN can be identified by this method. In the case of selective detection of the interface, the

depth of analysis has to be on the order of a nanometre to obtain data with reduced bulk information, even in the direct interface measurements or for the surface during the process in progress. Therefore, the oxide film has to be thinned to allow the underlying GaN to be detected in the case of GaN with an oxide film.

However, in the EXAFS measurements of Ga, the analysis depth in general electron yield is deep (50–100 nm) because of the high energy of the Ga *K*-edge (Girardeau *et al.*, 1992; Schroeder *et al.*, 1995). Under the total reflection condition of the incident X-ray, the analysis depth is shallow; however, a significantly sized area is required for analysis in turn (Kataoka *et al.*, 2012). In the Ga *L*-absorption edge with low energy, the analysis depth is likewise shallow; however, the EXAFS analysis with Fourier transformation is difficult to perform, as Ga *L*1, *L*2 and *L*3 absorption edges are adjacent to each other (*L*1–*L*2: 156 eV; *L*2–*L*3: 27 eV), and thus the EXAFS oscillations overlap (Rabe *et al.*, 1979).

We studied surface-sensitive techniques of EXAFS by detecting Auger electrons escaping from sample surfaces (Isomura *et al.*, 2016, 2017, 2018). EXAFS spectra are obtained during the energy sweep of the incident X-ray by monitoring the intensity of Auger electrons using the electron monochromator. Even at the *K*-edge, *LMM* Auger electrons with low energies cascade from the *KLL* Auger process, originating from *K*-shell absorption (Busch *et al.*, 1994). The inelastic mean free path (IMFP) of Ga *LMM* Auger electrons is 2.3 nm in comparison with 11.3 nm of Ga *KLL* Auger electrons, obtained for GaN by using the algorithm of Tanuma, Powel and Penn (TPP-2M) (Tanuma *et al.*, 2011), which corresponds to the analysis depth. Hence, analysis depth on the order of a nanometre can be expected by detecting *LMM* Auger electrons.

In this study, we propose a surface-sensitive measurement of Ga *K*-edge EXAFS by detecting Ga *LMM* Auger electrons with low energies for GaN. In addition, the analysis depth is investigated using a thermally oxidized GaN with an oxide film of defined thickness.

2. Experimental

Experiments were performed at the BL16XU beamline of the Super Photon Ring 8 GeV (SPring-8) (Hirai *et al.*, 2004) with a 1436 m circumference electron storage ring, operated at 8 GeV electron energy and 100 mA current.

Quasi-monochromatic light from an undulator was monochromated by a Si(111) double-crystal monochromator. The beam size at the sample position was 0.3 mm × 0.05 mm (horizontal × vertical). The electron analyzer (R4000, Scienta Omicron GmbH) comprised a concentric hemispherical analyzer with a mean radius of 200 mm, a combined pre-retarding second-order focusing-lens system and a two-dimensional event-counting detector equipped with a multichannel plate, a phosphor screen and a CCD camera. The pass energy was 200 eV, resulting in the energy window being 20 eV in fix mode, which allows quick acquisitions. The total energy resolution was 1 eV, measured by the Fermi edge of Au at 10 keV X-ray energy. The lens axis of the analyzer was oriented perpendicular to the incident X-ray beam and parallel to the polarization vector. The incidence angle relative to the sample surface was set to 10° and the take-off angle of the analyzed electrons was 80°. Auger electrons emitted from the sample surface during X-ray energy sweeps were detected by the electron analyzer. Bulk measurements were obtained in terms of the total electron yield (TEY) by detecting the sample's drain current. The base pressure of the main chamber was approximately 1×10^{-6} Pa.

The sample used herein was a GaN(0001) single-crystal substrate. The thermally oxidized GaN substrate was also used for investigation of the analysis depth. To this end, it was annealed at 900°C for 5 min in the presence of O_2 under ambient pressure in a ramp-heating furnace. The thickness of the oxide film was 10 nm. Moreover, a β-Ga_2O_3(-201) single crystal substrate was used to obtain a standard spectrum of gallium oxide.

3. Results and discussion

Fig. 1 shows Ga *KLL* and *LMM* Auger electron spectra for GaN irradiated with X-rays. The X-ray energies below and above the *K*-edge are set to 10 300 eV and 10 400 eV, respectively, as the energy of the Ga *K*-edge is 10 367 eV (Brendt *et al.*, 2009).

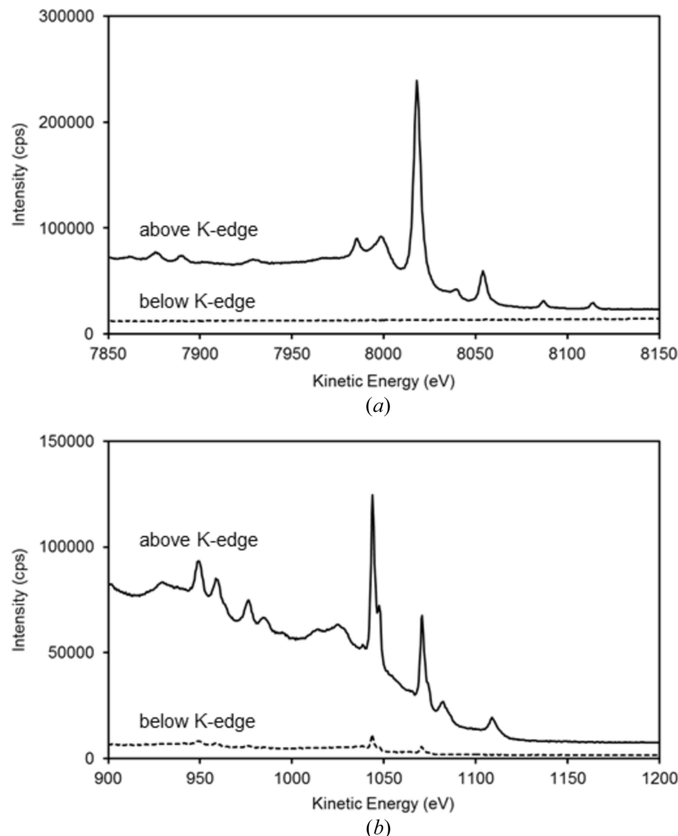

Figure 1
(*a*) Ga *KLL* and (*b*) Ga *LMM* Auger electron spectra of GaN irradiated with X-rays. The dashed and solid lines indicate the spectra below (X-ray energy of 10 300 eV) and above (10 400 eV) the Ga *K*-edge, respectively.

In the *KLL* Auger spectra of Fig. 1(*a*), many peaks can be observed ∼8000 eV above the *K*-edge, although no peak is present before. Shirley (1973) predicted, by theoretical calculation, that Ga *KLL* Auger peaks appear at ∼8000 eV, which is in agreement with our result. In contrast, in the *LMM* Auger spectra of Fig. 1(*b*), several small peaks are observable at ∼1000 eV below the *K*-edge. These peaks are caused by the *L*-absorption, as its energy is 1100–1300 eV and it is lower than 10 300 eV (below the *K*-edge). Above the *K*-edge, the intensity of those peaks increased and several more peaks appeared around 1000 eV. Antonides *et al.* (1977) reported, by experimental measurement, that Ga *LMM* Auger peaks appear around 1000 eV, which is in agreement with our results. Moreover, the intensity of *LMM* Auger peaks was not small, at approximately half the magnitude of those of *KLL* (Fig. 1).

Fig. 2 shows Ga *K*-edge EXAFS spectra for GaN, obtained by detecting Ga *KLL* and *LMM* Auger electrons (hereafter referred to as *KLL* and *LMM* detections, respectively), along with the analytical results derived from the EXAFS spectra. The peaks, whose intensities stood out significantly against the background, were observed at the energies of 8018 eV and 1071 eV for *KLL* and *LMM* detections, respectively (Fig. 1). These peaks' intensities, integrated with a width of 20 eV, were recorded during X-ray energy sweeps. EXAFS oscillations were extracted from the EXAFS spectra as a function of wavevector and their Fourier transforms were derived. We used the *ATHENA* data processing suite package to perform these extractions and derivations (Ravel & Newville, 2005). The Fourier transformations were performed at a *k*-range from 3.0 to 9.7 with a relatively good signal-to-noise ratio and they indicate the radial-structure functions (RSFs) of the Ga atoms. Note that the interatomic distances revealed by RSFs are shorter than the actual values because the factors of phase shift are included in RSFs.

The edge energies of EXAFS spectra for *KLL* and *LMM* detections are present at 10 367 eV in both cases [Fig. 2(*a*)], which is in agreement with the value from the conventional transmission measurement of GaN reported by Brendt *et al.* (2009). In the Fourier transforms [Fig. 2(*c*)], the first nearest-neighbor peak at 1.4 Å and the second-nearest-neighbor peak at 2.9 Å indicate N and Ga atoms, respectively. These peak positions are in agreement with the values reported by Brendt *et al.* (2009). Hence, we can assume that the EXAFS analysis detects *LMM* Auger electrons that indeed originate from the *K*-shell absorption.

The intensity of the second-nearest-neighbor peak for *LMM* detection is 12.0% lower than that for the *KLL* detection [Fig. 2(*c*)]. The peak intensity in Fourier transforms reflects the coordination number and the local structural order around the target atoms (Teo & Joy, 1980). Therefore, the result for *LMM* detection suggests a low coordination number and/or low structural order around Ga atoms. The intensity of Auger electrons decreases exponentially with the electron escape depth. The contribution of the first (surface) layer (∼0.3 nm) relative to bulk is estimated to be ∼12% for the IMFP of 2.3 nm (*LMM* detection). This contribution is in good agreement with the above-mentioned intensity reduction of

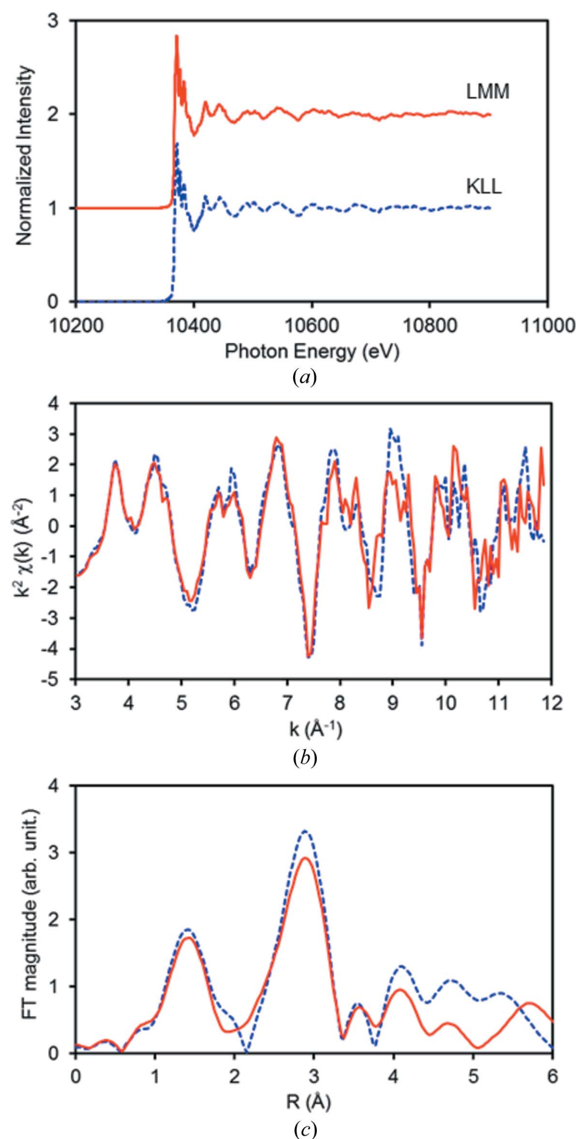

Figure 2
(*a*) Ga *K*-edge EXAFS spectra for GaN, obtained by detecting Ga *KLL* and *LMM* Auger electrons; (*b*) EXAFS oscillation as a function of wavevector, extracted from the EXAFS spectra; and (*c*) Fourier transforms derived from EXAFS oscillations, without consideration of phase shifts. The dashed blue and solid red lines indicate *KLL* and *LMM* detections, respectively.

12.0%. In contrast to bulk, the surface can generally have dangling bonds or hydrogen terminations *etc.* As a result, the surface could indicate an apparent low coordination number and/or low structural order.

The analysis depth of the *LMM* detection was quantitatively assessed. Fig. 3 shows the Ga *K*-edge X-ray absorption near-edge structure (XANES) spectra obtained by *KLL* and *LMM* Auger electron detection for the thermally oxidized GaN (the oxide-film thickness is ∼10 nm), along with the TEY-XANES spectra of GaN and Ga_2O_3.

The XANES spectrum of *KLL* detection for the oxidized GaN is similar to that for GaN with regard to the spectral shape (Fig. 3). The linear combination fitting (LCF) for the spectrum of *KLL* detection with the standard spectra of GaN and Ga_2O_3 was performed using *ATHENA* (Ravel &

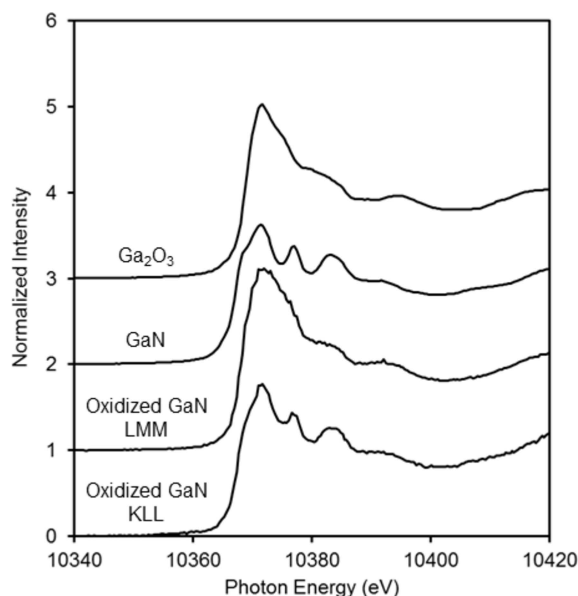

Figure 3
Ga *K*-edge XANES spectra from detected Ga *KLL* and *LMM* Auger electrons for thermally oxidized GaN, plotted along with TEY-XANES spectra of GaN and Ga_2O_3.

Newville, 2005), yielding the ratio of GaN/Ga_2O_3 = 0.70/0.30 (the *R* factor, which is a mean-square sum of the misfit at each data point, is 0.002). Note that the ratio does not indicate the amount ratio because the fitting was performed using the normalized spectra. The absorbances (absolute intensities at 10 400 eV) between GaN and Ga_2O_3 were different and their ratio (GaN/Ga_2O_3) was 1.65. Hence, the amount ratio of GaN/Ga_2O_3 is calculated to be 0.59/0.41. However, the contribution of electrons from the surface layer with a thickness of 10 nm (assuming the Ga_2O_3 film in this study) is estimated to be 0.59 for *KLL* Auger electrons (Hofmann, 1983), indicating a disagreement with the fraction of Ga_2O_3 (0.41) in the amount ratio, although in the case of a single material (no large difference in a two-layer model) of the Ga_2O_3 film/GaN substrate. This disagreement may be caused by the structure being different from the single crystal of Ga_2O_3 (described later). The structure with low density, *e.g.* defects (vacancies) and disorder, can lead to the lower fraction of Ga_2O_3.

In contrast, the XANES spectrum of the *LMM* detection for the oxidized GaN is similar to that of Ga_2O_3 with respect to the spectral shape; however, a slight broadening is observed in the former (Fig. 3). LCF for the spectrum of *LMM* detection with the standard spectra of GaN and Ga_2O_3 was performed (Ravel & Newville, 2005), yielding the ratio of GaN/Ga_2O_3 = 0.00/1.00 (the amount ratio is also 0.00/1.00) and a non-perfect fit with a considerable *R* factor of 0.025. This discrepancy may be caused by the difference between thermal oxidation and the single crystal of Ga_2O_3. The IMFP of Ga *LMM* Auger electrons is 2.3 nm (Tanuma *et al.*, 2011), which gives an information depth of 7 nm. The contribution of electrons from the surface layer with a thickness of 10 nm (assuming the Ga_2O_3 film in this study) is estimated to be 0.99 for *LMM* Auger electrons (Hofmann, 1983), indicating good agreement with the fraction of Ga_2O_3 (1.00). By investigating the thermally oxidized GaN with an oxide-film thickness of 10 nm, we can assume that the analysis depth is below 10 nm, where the depth reaching 1/*e* intensity is 2.3 nm, for the EXAFS analysis detecting Ga *LMM* Auger electrons originating from the Ga *K*-shell absorption.

4. Conclusions

We proposed a surface-sensitive measurement of Ga *K*-edge EXAFS by detecting Ga *LMM* Auger electrons with low energies at the Ga *K*-edge absorption for GaN. We were able to observe the Ga *K*-edge EXAFS oscillation by detecting Ga *LMM* Auger electrons. In the Fourier transform derived from the EXAFS oscillation, the first- and second-nearest-neighbor peaks were in agreement with the reported values of GaN in position, indicating the validity of the *K*-edge EXAFS analysis detecting *LMM* Auger electrons generated in the Auger cascade process following *K*-shell absorption. Investigation of a thermally oxidized GaN layer with an oxide film of ~10 nm thickness revealed the analysis depth at less than 10 nm, where the depth reached by 1/*e* intensity is 2.3 nm. Hence, this *K*-edge EXAFS technique detecting *LMM* Auger electrons enables the analysis of local atomic structure in material surfaces and thus contributes to the development of GaN power semiconductor devices.

Acknowledgements

The authors are grateful to Mr Masatake Machida of Scienta Omicron Inc. for his advice regarding the measurement conditions. Synchrotron radiation measurements were performed at the BL16XU of SPring-8 with the approval of the Japan Synchrotron Radiation Research Institute (Proposal Nos. 2018B5071 and 2019A5071).

References

Antonides, E., Janse, E. C. & Sawatzky, G. A. (1977). *Phys. Rev. B*, **15**, 1669–1679.
Brendt, J., Samuelis, D., Weirich, T. E. & Martin, M. (2009). *Phys. Chem. Chem. Phys.* **11**, 3127–3137.
Busch, F., Doppelfeld, J., Güunther, C. & Hartmann, E. (1994). *J. Phys. B At. Mol. Opt. Phys.* **27**, 2151–2160.
Chakroun, A., Maher, H., Alam, E. A., Souifi, A., Aimez, V., Arès, R. & Jaouad, A. (2014). *IEEE Electron Device Lett.* **35**, 318–320.
Girardeau, T., Mimault, J., Jaouen, M., Chartier, P. & Tourillon, G. (1992). *Phys. Rev. B*, **46**, 7144–7152.
Hirai, Y., Yasuami, S., Kobayashi, A., Hirai, Y., Nishino, J., Shibata, M., Yamaguchi, K., Liu, K.-Y., Kawado, S., Yamamoto, T., Noguchi, S., Takahashi, M., Konomi, I., Kimura, S., Hasegawa, M., Awaji, N., Komiya, S., Hirose, T., Ozaki, S., Okajima, T., Ishikawa, T. & Kitamura, H. (2004). *Nucl. Instrum. Methods Phys. Res. A*, **521**, 538–548.
Hofmann, S. (1983) *Practical Surface Analysis by Auger and X-ray Photoelectron Spectroscopy*, edited by D. Briggs & M. P. Seah, pp. 141–179. Chichester, UK: John Wiley & Sons Ltd.
Isomura, N., Kosaka, S., Kataoka, K., Watanabe, Y. & Kimoto, Y. (2018). *Jpn. J. Appl. Phys.* **57**, 060308.
Isomura, N., Murai, T., Nomoto, T. & Kimoto, Y. (2017). *J. Synchrotron Rad.* **24**, 445–448.

Isomura, N., Murai, T., Oji, H., Nomoto, T., Watanabe, Y. & Kimoto, Y. (2016). *Appl. Phys. Expr.* **9**, 101301.
Kachi, T. (2014). *Jpn. J. Appl. Phys.* **53**, 100210.
Kataoka, K., Kimoto, Y., Horibuchi, K., Nonaka, T., Takahashi, N., Narita, T., Kanechika, M. & Dohmae, K. (2012). *Surf. Interface Anal.* **44**, 709–712.
Kim, S., Hori, Y., Ma, W.-C., Kikuta, D., Narita, T., Iguchi, H., Uesugi, T., Kachi, T. & Hashizume, T. (2012). *Jpn. J. Appl. Phys.* **51**, 060201.
Nakano, Y., Kachi, T. & Jimbo, T. (2003). *Appl. Phys. Lett.* **83**, 4336–4338.
Rabe, P., Tolkiehn, G. & Werner, A. (1979). *J. Phys. C. Solid State Phys.* **12**, 899–905.
Ravel, B. & Newville, M. (2005). *J. Synchrotron Rad.* **12**, 537–541.
Schroeder, S. L. M., Moggridge, G. D., Ormerod, R. M., Rayment, T. & Lambert, R. M. (1995). *Surf. Sci.* **324**, L371–L377.
Shirley, D. A. (1973). *Phys. Rev. A*, **7**, 1520–1528.
Stern, E. A. & Heald, S. M. (1983). *Handbook on Synchrotron Radiation*, Vol. 1*B*, edited by E. E. Koch, p. 955. Amsterdam: North-Holland.
Tang, K., Huang, W. & Chow, T. P. (2009). *J. Elec Materi*, **38**, 523–528.
Tanuma, S., Powell, C. J. & Penn, D. R. (2011). *Surf. Interface Anal.* **43**, 689–713.
Teo, B. K. & Joy, D. C. (1980). *EXAFS Spectroscopy*. New York: Plenum.
Trivedi, M. & Shenai, K. (1999). *J. Appl. Phys.* **85**, 6889–6897.